Regular Article

PHYSICAL CHEMISTRY RESEARCH
Published by the
Iranian Chemical Society
www.physchemres.org
info@physchemres.org

Phys. Chem. Res., Vol. 5, No. 1, 167-183, March 2017
DOI: 10.22036/pcr.2017.39484

Sensitivity of Perfect and Stone-Wales Defective BNNTs Toward NO Molecule: A DFT/M06-2X Approach

H. Roohi* and M. Jahantab

Department of Chemistry, Faculty of Science, University of Guilan, Rasht, Iran

(Received 17 June 2016, Accepted 4 November 2016)

The monitoring and controlling of environmental pollutions are very important in biological and industrial processes, and a great interest is growing with the development of suitable gas-sensitive materials and hazardous chemical removal devices. In this work, the highly parameterized, empirical exchange-correlation functional M06-2X was employed to investigate the electronic sensitivity of perfect (PS) and Stone-Wales defective (SW) BNNTs toward NO molecule. A detailed analysis was performed on the structural and electronic properties, reactivity and electron density of the states of various NO-BNNT complexes. Our results reveal that the NO adsorption on the outer and inner surface sites of both PS and SW nanotubes is energetically favorable and unfavorable, respectively. The electronic property analysis indicates that the formation of Stone-Wales defect reduces the energy gap of BNNT and increases its electrical conductivity. In addition, adsorption of NO on the both PS- and SW-BNNTs reduces the energy gap of the nanotubes and increases their electrical conductance, which could serve as a signal for gas sensor. In addition, adsorption of NO radical on both BNNTs decreased the work function and so increased the electron emission field of the BNNT surfaces. The present results can provide useful guidance to develop modified BNNTs as a NO sensor.

Keywords: M06-2X, Adsorption, Boron nitride nanotube, Stone-Wales defect, Energy gap, Electronic properties

INTRODUCTION

Boron nitride nanotubes (BNNTs) as an important class of inorganic nanotubes have attracted the significant attention since their theoretical prediction in 1994 [1-2]. Compared with the carbon nanotubes (CNTs), electronic properties of BNNTs are independent of the tube diameter, chirality and number of shells [3]. Because of their superior chemical stability, electronic and optical energy gap properties [4], BNNTs have many interesting potential applications in optical sensors [5], lasing action [6], hydrogen storage [7] and nanoelectronic devices. The large energy gap and chemical inertness impose great restriction on the wider applications of BNNTs. Therefore, various types of defects can be formed in BNNTs (such as vacancies, foreign atom substitutions, or topological defe) in the process of experimental growth or modifications [8-10]. The Stone-Wales defect [11] is formed by 90° rotation of B-N bond at the hexagonal arrangement that generates two unfavorable homo-elemental (B-B and N-N) bonds [12]. Formation of B-B and N-N bonds increases the total energy of the system [13]. The existence of SW defect may modify the reactivity and electronic as well as mechanical properties of BNNTs.

Nitric oxide (NO) is a toxic free radical gas known as a byproduct in almost all types of organisms, ranging from bacteria to plants, fungi, and animal cells [14]. Selective reduction of NO in oxidizing atmospheres has recently received much attention, because it has potential as a practical measure to remove NO_x emitted from diesel and lean burn engines [15]. A very different area, where NO sensing is also required is in the medical industry, specifically in breath analysis for diagnosis of respiratory ailments [16]. Therefore, reliable and low-cost NO sensors

*Corresponding author. E-mail: hroohi@guilan.ac.ir

with high selectivity and sensitivity have been required for environmental safety. Chang *et al*. [16] have tested NO sensors that are significantly smaller than previously demonstrated sensors. Recently, there are reports on the adsorption of NO molecule on nanotubes. For example, if defected SWCNTs is embedded in physiological systems, can serve as a sensor for biological NO [17]. The chemisorption process of NO and N_2O molecules on carbon edge sites and the subsequent reduction of these gases to N_2 were simulated by using ab initio method [18]. Yates et al. [19] have studied the physical adsorption of NO on purified single-walled carbon nanotubes at low temperatures by means of transmission infrared spectroscopy. Rafati *et al*. [20] investigated the adsorption of NO on the armchair (4,4), (5,5), (6,6) and (7,7) carbon nanotubes at B3LYP/3-21G(d,p) level of theory. They found that one NO molecule can be physisorbed on the surface of CNTs endothermically. Udhayakumar *et al*. [21] utilized theoretical approach to study the NO adsorption on the top surface of C, BC, and SiC nanotubes, and found that BCNT and SiCNT are good candidates for gas sensor applications.

An effective method of sensing and removing the NO molecule is still needed. Single-walled BNNTs can also act as a chemical sensor with higher sensitivities, lower limits of detection and faster response time for NO molecule if their electronic conductance changed upon exposure to gas molecule. Using a theoretical method based on first principles, the chemisorption of NO and NNO molecules on SiCNTs, CNTs and BNNTs was investigated by Kang et al. [22]. They found that NO and NNO molecules can be chemisorbed on SiCNTs with an appreciable binding energy and that this is not the case for either CNTs or BNNTs. The electronic and structural properties of NO adsorbed on C-doped BNNT have been investigated by first principle calculations [23]. The results showed that pure BNNT presents a low sensitivity to NO, whereas C-doped BNNT can improve the interaction between NO molecules and BNNT. Xie *et al.* [24] studied the adsorption of NO molecule on transition metals (TM = V, Cr, Mn, Fe, Co or Ni) doped (8,0) BNNT using first principle calculations. They found that the NO adsorption on TM-doped BNNT is exothermic. Recently, we investigated adsorption sensitivity of C-doped Stone-Wales defective BNNTs toward NO radical [25]. In this study, interactions between NO molecule and perfect (PS) BNNT as well as Stone-Wales defected BNNT (SW) were investigated using the M06-2X density functional calculations. In addition, structural and electronic properties of the pure and complexed structures of PS and SW nanotubes were determined to provide useful information for designing new gas sensors and nano-electronic devices.

Computational Details

To investigate the adsorption behavior of NO radical on the BNNTs, two finite-length zigzag (6,0) nanotubes ($B_{36}N_{36}H_{12}$) including perfect and Stone-Wales defected BNNT were selected. To avoid the boundary effects, atoms at the open ends of the tubes were saturated by hydrogen atoms. The average length of optimized PS- and SW-BNNTs was computed to be 11.574 and 11.390 Å, respectively. An ONIOM methodology [26-27] was used to study the effect of Stone-Wales defect on adsorption of NO radical on BNNTs. In our previous study (see Ref. [25]), to confirm the results obtained using ONIOM model, adsorption energies of 2C-doped SW-BNNT complexes were calculated after full optimization. The results of full optimization were in good agreement with those of ONIOM approach. For an instant, the adsorption energies for H and J complexes were 5.1 and -11.5 kcal mol^{-1}, respectively, that were very close to those found using the ONIOM method (4. 6 and -11.5 eV). ONIOM approach [28-29] has clear advantages for modeling nanoscale systems. Using this technique, it is possible to model a large system by applying a high-level quantum mechanical theory to the immediate region of interest and a lower level of theory, such as semiempirical or molecular mechanics, to the rest of the system. It can avoid the computationally prohibitive step of applying high-level theory to a system with many atoms while still yielding accurate results. In fact, ONIOM calculations have been shown to successfully model both covalent and noncovalent interactions involving nanotubes [27,30-41]. In ONIOM approach, the system is divided into a reactive part, which is treated at an appropriately high computational level, while the remainder of the system is included at a less expensive lower level of theory. This provieds an appropriately high level of accuracy for the reactive part of the system, while reducing the computational cost for the smaller part using an expensive

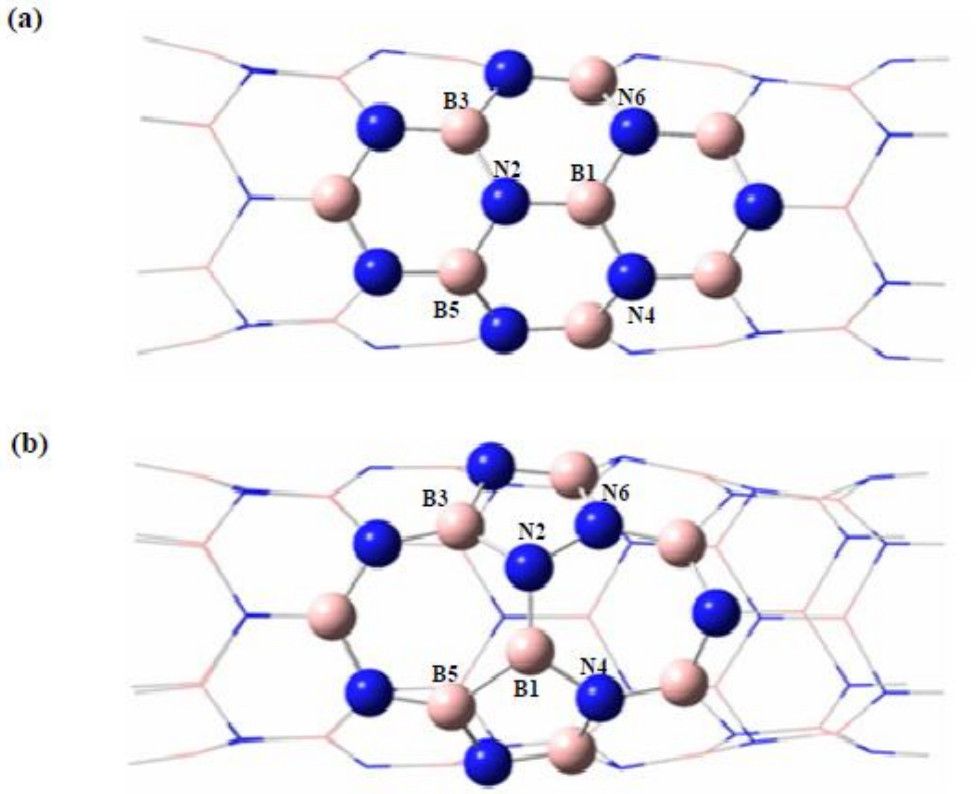

Fig. 1. ONIOM models of (a) perfect (6,0) tube model and (b) defective (6,0) tube model containing a Stone-Wales defect. Ball and bond type structures represent the higher layer and wire frame represents the low layer. Pink and blue balls represent boron and nitrogen atoms, respectively. (For interpretation of the references to color in this figure legend, the reader is referred to the web version of this article).

method [30]. In the ONIOM methodology used in this work, small part of the nanotube including the NO molecule and the atoms around the adsorbing sites denoted by the big balls (high theoretical level) was treated using the M06-2X functional [42] with the 6-31++G(d,p) basis set [43-45], while rest of the system (low theoretical level) was treated using the semi-empirical PM6 method [46] (see Fig. 1). Single point calculations have been performed on the optimized structures at the M06-2X/6–31++G(d,p) level of theory to obtain the most reliable energies.

Electronic chemical potential, chemical hardness and softness are known as global reactivity descriptors [47-48]. The relation of chemical potential (μ) with the electronegativity (χ) could be written as

$$\mu = -\chi = -\frac{1}{2}(I + A) \tag{3}$$

The global chemical hardness (η) is defined as

$$\eta = \frac{1}{2}(I - A) \tag{4}$$

where I and A are the first ionization energy and electron affinity, respectively. The most widely used theory by chemists is the molecular orbital (MO) theory. This can be readily performed within the limitations of Koopmans' theorem [49].The orbital energies of the frontier orbitals are given by [50]

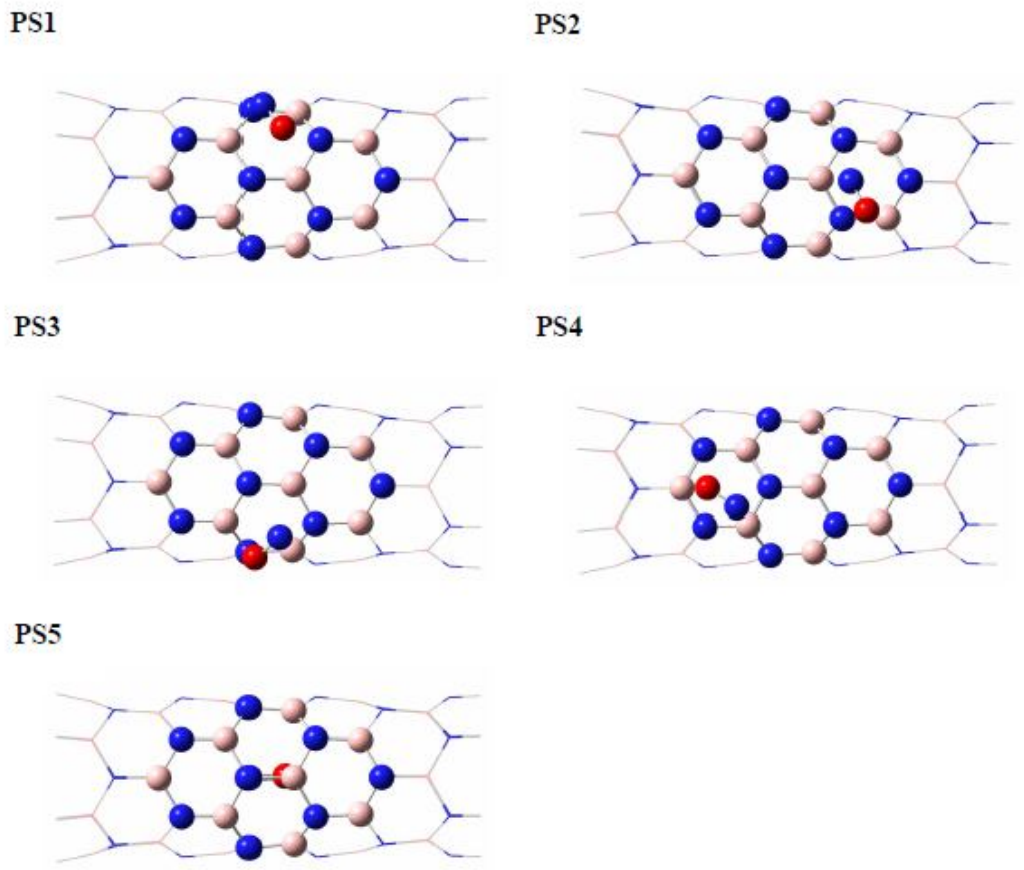

Fig. 2. Optimized structures of PS-BNNTs. Ball and bond type structures represent the higher layer and wire frame represents the low layer. Pink, blue and red balls represent boron, nitrogen and oxygen atoms, respectively. (For interpretation of the references to color in this figure legend, the reader is referred to the web version of this article).

$$-\varepsilon_{\mathrm{LUMO}} = A \tag{5}$$

$$-\varepsilon_{\mathrm{HOMO}} = I \tag{6}$$

$$\mu = -\chi = \frac{1}{2}(\varepsilon_{\mathrm{HOMO}} + \varepsilon_{\mathrm{LUMO}}) \tag{7}$$

$$\eta = \frac{1}{2}(\varepsilon_{\mathrm{LUMO}} - \varepsilon_{\mathrm{HOMO}}) \tag{8}$$

The chemical softness (S) is defined by

$$S = \frac{1}{2\eta} \tag{9}$$

Parr *et al*. [51] have defined a new descriptor to quantify the global electrophilic power of the molecule as electrophilicity index (ω). This reactivity index measures the stabilization energy when the system acquires an additional electronic charge from the environment.

$$\omega = \frac{\mu^2}{2\eta} \tag{10}$$

The maximum amount of electronic charge (ΔN_{max}) [51], that the system may accept, is defined as following equation

$$\Delta N_{\max} = \frac{-\mu}{\eta} \tag{11}$$

while the quantity defined by Eq. (10) describes the

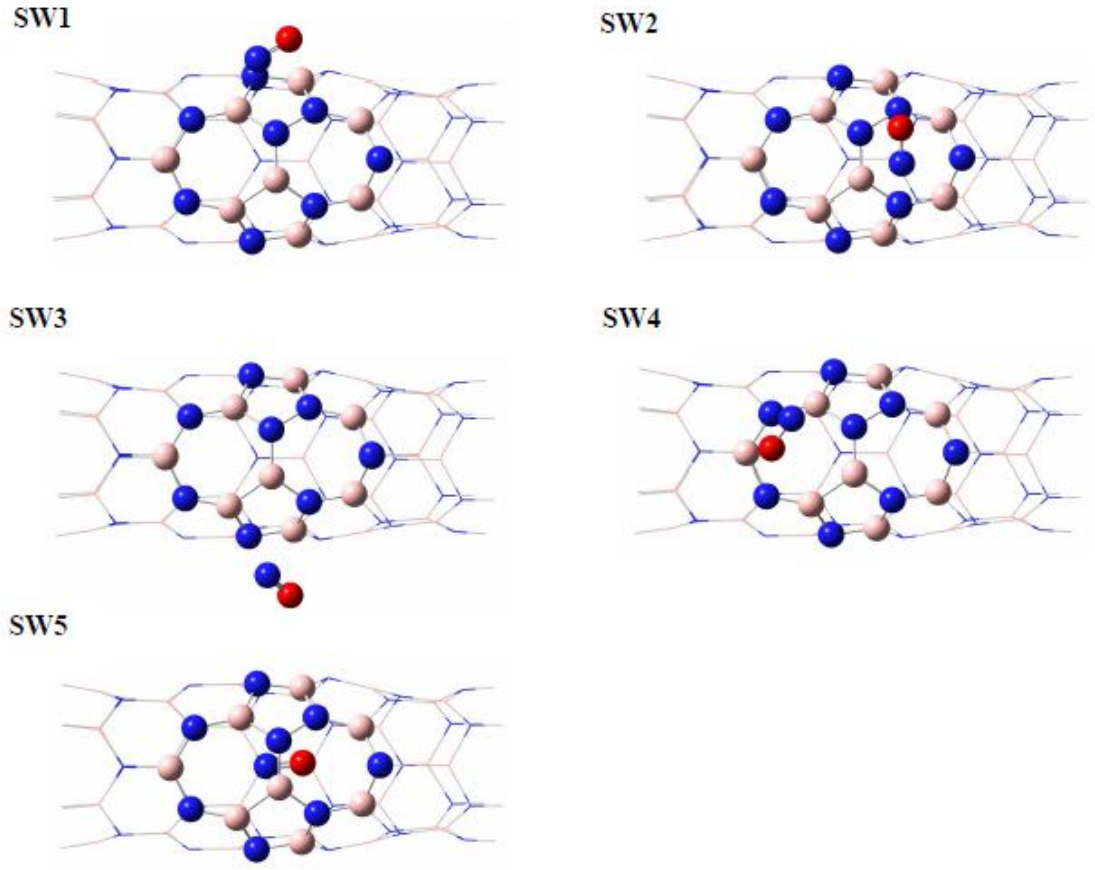

Fig. 3. Optimized structures of SW-BNNTs. Ball and bond type structures represent the higher layer and wireframe represents the low layer. Pink, blue and red balls represent boron, nitrogen and oxygen atoms, respectively. (For interpretation of the references to color in this figure legend, the reader is referred to the web version of this article).

propensity of the system to acquire additional electronic charge from the environment, and the quantity defined in Eq. (11) describes the charge capacity of the molecule [52]. All calculations have been performed using the GAUSSIAN-09 [53] and GAMESS program packages [54]. The plots of Density of states (DOS) have been obtained using GaussSum software [55].

RESULTS AND DISCUSSION

Energies and Geometries

The optimized structures of PS- and SW-BNNTs are displayed in Figs. 2 and 3, and the selected geometrical parameters of all optimized structures are given in Table 1. The circumferences of the zigzag nanotube consist of one type atom, either N or B atoms; if one of the ends is formed by N atoms, the other end is formed by B ones. Diameters of the N-terminated and B-terminated nanotubes are 5.111 and 4.836 Å in pure PS and 5.101 and 4.836 Å in pure SW, respectively. The tube diameter at the end of N-terminated is greater than that of B-terminated in both nanotubes. Stone-Wales defect generates structural deformation in BNNT and changes the local curvature at defect site. The N and B atoms in the 7-7 ring fusion of the defective tube model move outward from the tube surface. Diameters of the middle rings of pure PS- and SW-BNNTs are computed about 5.000 and 5.207 Å, respectively. There are two types of B-N bonds in perfect zigzag BNNT; the B-N bonds

Table 1. The Selected Geometrical Parameters (Å) of NO Adsorption on Perfect and Defective (6,0) BNNTs. The Data in the Parenthesis Correspond to the NO Monomer

Models	B1-N2	B1-N4	B3-N2	N2-N6	B1-B5	O-N
Pure PS	1.449	1.467	1.471			(1.147)
PS1	1.447	1.466	1.472			1.146
PS2	1.450	1.469	1.471			1.146
PS3	1.448	1.470	1.469			1.147
PS4	1.450	1.467	1.472			1.148
PS5	1.455	1.474	1.493			1.158
Pure SW	1.439	1.470	1.503	1.454	1.724	
SW1	1.440	1.469	1.507	1.452	1.724	1.147
SW2	1.440	1.471	1.500	1.453	1.725	1.146
SW3	1.439	1.471	1.503	1.454	1.723	1.146
SW4	1.439	1.469	1.506	1.453	1.725	1.148
SW5	1.472	1.471	1.516	1.441	1.733	1.158

Table 2. Adsorption Energies (ΔE_{ads}), HOMO Energy (E_{HOMO}), LUMO Energy (E_{LUMO}) and HOMO-LUMO Energy Gap (E_{L-H}) of Zigzag BNNTs

Models	ΔE_{ads} (eV)	E_{HOMO} (eV)	E_{LUMO} (eV)	E_{L-H} (eV)
Pure PS		-8.225	-1.577	6.647
PS1	-0.170	-7.842	-1.577	6.264
PS2	-0.166	-7.776	-1.575	6.201
PS3	-0.161	-7.813	-1.573	6.241
PS4	-0.167	-7.815	-1.577	6.238
PS5	1.859	-8.150	-2.625	5.525
Pure SW		-7.880	-1.511	6.370
SW1	-0.155	-7.637	-1.511	6.126
SW2	-0.159	-7.546	-1.509	6.037
SW3	-0.151	-7.771	-1.506	6.264
SW4	-0.157	-7.793	-1.502	6.291
SW5	0.909	-7.916	-2.333	5.584
NO		-7.938	-1.459	6.479

around and along the tube axis. On the other hand, when the Stone-Wales defect is created, three types of B-N bonds can be found: zigzag and axial B-N bonds and one B-N bond orthogonal to the tube axis (bond connecting the two pentagons and two heptagons). The optimized B1-N2 bond length (1.439 Å) in the 7-7 ring fusion of the defective tube model is shorter than the B1-N2 bond in the perfect tube model (1.449 Å), indicating a less reactivity of this bond in defective tube compared to perfect one. The zigzag B1-N4 and B3–N2 bond lengths in pure PS and SW nanotubes are (1.470, 1.503 Å) and (1.467, 1.471 Å), respectively, implying a greater reactivity of the defective tube in these sites. Also, in the presence of SW defect, one B-B bond and one N-N bond are produced with the bond lengths of 1.724 and 1.454 Å, respectively. The B-B bond length is greater than N-N one, due to the longer covalent radius of B (0.84 Å) than that of N (0.71 Å).

Formation of B-B and N-N bonds in BNNT is unfavorable energetically [56-57]. The structural instability induced by a transformation from a normal B-N bond to frustrated B-B and N-N bonds is known as the bond frustration effect [8,58-59]. The bond length measurements also show that the bond frustration effect is caused mainly by the local strain because a change in bond lengths occurs only for B-N bonds near the Stone-Wales defect site [8]. The energies required to form the Stone-Wales defect (defect formation energy) is defined as: $E_F = E_{SW} - E_{PS}$, where E_{SW} and E_{PS} are the total energy of the pure SW- and PS-BNNTs, respectively. Li *et al*. [57] reported that the energies of forming Stone-Wales defects in a series of zigzag (n,0) (n = 7, 8, 10, 12, or 15) BNNTs depend not only on the defect orientations but also on the tube diameter. They found that the defect formation energies increase with increasing tube diameters. The calculated defect formation energy is 4.22 eV for (6,0) BNNT. Positive E_F denotes an endothermal procedure for the formation of a defect.

The binding energy (BE) per atom for SW and PS tubes was calculated according to the following formula:

$$BE = \frac{[aE_B + bE_N + cE_H] - [E_{BaNbHc}]}{a + b + c} \quad (1)$$

where a, b and c are the number of B, N and H atoms and E_B, E_N and E_H are the ground state total energies of B, N and H atoms, respectively. E_{BaNbHc} is the total energy of the optimized clusters representing the nanotubes. The calculated BE value for pure SW nanotube (7.14 eV) is smaller than BE of pure PS one (7.19 eV). Formation of B-B and N-N bonds in SW-BNNT decreases the BE value.

NO Adsorption on the BNNTs

To find the most stable configurations of NO adsorbed on BNNTs, one NO molecule as N-down, O-down and side on (*i.e.* NO bond axis is parallel with the BN bonds) was located on the zigzag, axial and perpendicular B-N bonds at a certain distance of the tube. After optimization, four configurations PS1-4 and SW1-4 were obtained, as shown in Figs. 2 and 3. As can be seen in Fig. 2, NO in PS1-4 structures is placed on the hexagon rings of the perfect nanotube. For the SW1-4 configurations, NO is located above the pentagon and heptagon rings of SW−BNNT (see Fig. 3). All N-down and O-down modes of NO were converted to side on mode. In addition, NO molecules located on the inside of BNNTs have been explored. For structures of SW5 and PS5, NO is located inside of SW and PS nanotubes, respectively.

The complex formation leads to the structural changes in NO molecule. For the free NO molecule, the optimized N-O bond length is 1.147 Å. Upon complex formation, N-O bond length in SW1, SW4, SW5, PS3, PS4 and PS5 increases and in SW2, SW3, PS1 and PS2 decreases, slightly. The NO bond length and distance between NO moiety and BNNT (~3.000 Å) obtained by using the M06-2X functional reveals that a weak interaction occurs between NO molecule and PS- as well as SW-BNNTs. As can be seen in Table 1, B1-N2 bond length in both PS- and SW-BNNTs increases slightly (with the exception of PS1 and PS3). Upon adsorption of NO, the N-N bond length is reduced from 1.454 Å in pure tube to 1.452, 1.453, 1.454, 1.453 and 1.441 Å in SW1-SW5 BNNTs, respectively. Also, for the NO molecule adsorbed on SW-BNNTs the B-B bond lengths are longer than that pure SW-BNNT, with the exception of SW3.

The calculated adsorption energies are summarized in Table 2. The adsorption energy (E_{ads}) is defined as $E_{ads} = E_{(BNNT-NO)} - E_{(NO)} - E_{(BNNT)}$, where $E_{(BNNT–NO)}$ denotes the total energy of the combined NO-BNNT system, $E_{(BNNT)}$ is the energy of the isolated tube and $E_{(NO)}$ is the energy of a

single NO molecule. As shown in Table 2, E_{ads} for PS1-5 complexes is -0.170, -0.166, -0.161, -0.167 and 1.859 eV, respectively. Thus, favorable adsorption site of PS-BNNTs is located on the central hexagon ring and hexagon ring near the B-terminated is energetically more favorable than those of near N-terminated one. From these results, it can be predicted that the adsorption of NO on the outside of pure BNNT is an energetically favorable process. In contrast, adsorption on the inner surface of the tube is not energetically favorable.

The interaction between NO molecule and other nanotubes and the effects of these interactions on their properties are of great interest. For example, the adsorption energies of NO molecule on MgO [60] and SiC [22] nanotubes were estimated to be from -0.28 to -0.13 eV and -0.67 to -0.61 eV, respectively. Also, the calculated adsorption energies of NO molecule were -0.04 eV for (8,0) SWCNT [61] and -1.11, -2.44 and -2.49 eV for (8,0), (5,5) and (8,8) SWCNTs with vacancy defect [62], respectively. The comparison of non defective and defective CNTs shows that the adsorption energies in the former are smaller than those in the later.

El-Barbary *et al*. [63] have theoretically compared the adsorption energies of NO molecule on different chiralities of single-walled BNNTs. They have calculated adsorption energies of NO molecule on (5,0), (9,0), (5,5) and (6,6) BNNTs at B3LYP/6-31G(d,p) level of theory in the range of -0.20 to -0.23 eV, -0.14 to -0.26 eV, -0.11 to -0.16 eV and -0.17 to -0.19 eV, respectively. Also, calculations performed by using the Perdew-Burke-Ernzerhof (PBE) formulation of generalized gradient approximation (GGA) showed that the sensitivity of BNNT to NO gas increases upon doping namotube by transition metals (TM = V, Cr, Mn, Fe, Co and Ni) and carbon [23,24]. The adsorption energies of NO molecule on the pure and carbon doped BNNTs were -0.16 and -2.53 eV [23], respectively.

Gao *et al*. [22] found that the energies of interaction between NO and zigzag form of CNT and BNNT at PBEPBE/6-31G(d) level are significantly positive (1.710 to 2.03 eV for (8,0) CNT-NO and 1.57 to 1.62 eV for (8,0) BNNT-NO complexes). On the contrary to the Gao *et al*. results, our findings imply that adsorption of NO on PS-BNNTs is an exothermic process and thus it is estimated that they can be practically useful for the removal of NO molecule. It should be explained that the generalized gradient approximation (GGA) of PBE fails to describe dispersion interactions, which can be critical for noncovalent complexes. Dispersion interactions are inherently long-range electron correlation effects, which are not captured by the popular local or semilocal density functional. In addition to the DFT-D approaches, the highly parametrized empirical M05-2X and M06-2X functionals developed by Zhao and Truhlar have also shown promise for noncovalent interactions. According to Zhao and Truhlar, the M05 and M06 series of functionals implicitly account for "medium-range" electron correlation because of the way they are parameterized, and this is sufficient to describe the dispersion interactions within many complexes. In contrast to M05-2X and M06-2X, which are parameterized to fit a large number of experimental and higher-level theoretical data, all parameters in PBE (other than those in the underlying local spin density approximation) are physical constants. The M05-2X and M06-2X functionals have been used as benchmark methods for biologically relevant noncovalent interactions. Since, M06-2X functional provides significant improvements over traditional density functional (such as PBE) for the non-covalent interactions, thus, the results obtained by using M06-2X are more reliable than PBE one. It should be noted that only the electrostatic, exchange, and induction interactions are captured by PBE functional. Thus, this functional almost always underestimates the binding energy [42,64-71].

According to results given in Table 2, adsorption energies for SW1, SW2, SW3, SW4 and SW5 tubes are -0.155, -0.159, -0.151, -0.157 and 0.909 eV, respectively. The configuration of the lowest minimum energy corresponds to SW2, in which NO radical interacts with heptagon ring near the N-terminated of the BNNT (see Fig. 3). These results show that the interaction of NO radical with pentagon rings is less favorable than that of heptagon rings. Similar to PS-BNNT, the inner surface of SW-BNNT is not suitable for adsorption of NO molecule. It is predicted that the NO adsorption on the outer surface of PS and SW nanotubes occurs via exothermic process, while for internal site of both PS and SW nanotubes it occurs *via* an endothermic process. It can be noted that zero point energy correction may change above conclusion. Adsorption

energy of NO molecule on the armchair (4,4), (5,5), (6,6), and (7,7) SWCNTs was calculated at B3LYP/3-21G(d,p) level of theory in the range of 0.11-2.92 eV by Rafati *et al*. [20]. They found that the adsorption energies of interaction between NO and armchair form of CNT are positive. In contrast to the Rafati *et al*. results, our findings imply that adsorption of NO molecule on SW-BNNTs is an exothermic process. In addition, adsorptions of NO molecule on carbon doped (6,0) SW-BNNT at B3LYP/6-31+G(d) and M06-2X/6-31+G(d) levels of theory have been investigated by Roohi *et al*. [25]. The results reveal that the NO adsorption on the surface of C-doped SW-BNNTs is stronger than that on the pure and undoped SW-BNNTs.

Analysis of Electronic Properties

To understand the effect of NO adsorption on the electronic properties of BNNTs, highest occupied molecular orbital energy (E_{HOMO}), lowest unoccupied molecular orbital energy (E_{LUMO}) and the energy gap for PS- and SW-BNNTs are summarized in Table 2. Li *et al*. [57] reported that the formation of Stone-Wales defects in (8,0) BNNTs leads to new levels at the top of the valence band and at the bottom of the conduction band. These new levels reduced the BNNT energy gap by 0.21 and 0.47 eV for (8,0)-I and (8,0)-II, respectively. They found that the top valence bands originate mainly from the N atoms (especially those in N-N bonds) at the Stone-Wales defect sites. Conversely, the B atoms of B-B bonds dominate the bottom conduction bands. Thus, the energy gap reduction in these defective BNNTs is mainly due to the unfavorable N-N and B-B bonds in the Stone-Wales defects. Comparison of the results given in Table 2 indicates that the energy gap (energy gap = E_{LUMO} - E_{HOMO}) decreases slightly from 6.65 eV (PS) to 6.37 eV (SW). It is estimated that reduction of the energy gap in the presence of Stone-Wales defect increases its reactivity.

Table 2 also shows that the adsorption of NO radical on BNNTs decreases the energy gap of the PS- and SW-BNNTs. It is well known that one of the most important factors in HOMO/LUMO interactions is the energy difference between the HOMO of the nucleophile and the LUMO of the electrophile agent [72]. The results show that HOMO energy of the nucleophile agent (NO) is about -7.94 eV, and that of LUMOs for the adsorbents are given in Table 2, suggesting that the smallest values of energy gap for PS5 and SW5 nanotubes may come from their lower LUMO energy values (-2.62 and -2.33 eV, respectively). The relative reactivity of SW-BNNTs is in the order: SW5 > SW2 > SW1 > SW3 > SW4, whereas the relative reactivity of NO adsorbed on perfect nanotubes is in the order: PS5 > PS2 > PS3 = PS4 > PS1. Although the stability of PS tubes is greater than SW ones, the conductivity of PS is predicted to be smaller than SW tubes. This fact demonstrates the usefulness of PS- and SW-BNNTs for the development of sensors. In addition, decrease in the energy gap for internal sites of both PS and SW tubes are greater than corresponding outer surface sites.

The total densities of states (DOS) of an isolated NO molecule, pure BNNTs, and NO-BNNT systems at internal sites and also in the most stable configurations of outer surface sites (PS1 and SW2) were plotted to illustrate how the adsorption of NO affects the electronic structure of BNNTs (shown in Fig. 4). The DOS of these tubes shows changes due to NO adsorptions on the BNNTs. As a result, the adsorption of NO on the BNNTs decreases the energy gap of the pure BNNTs, and increases their electrical conductance. The electrical conductance of the semiconductor materials is related to energy gap value according to the following equation:

$$\sigma \propto \exp\left(\frac{-E_g}{2kT}\right) \quad (2)$$

where σ is the electrical conductivity, E_g is the energy gap, T is the temperature and k is the Boltzmann constant. According to this equation, smaller values of energy gap at a given temperature lead to higher electrical conductivity. According to the obtained results, adsorption of NO radical on both PS- and SW-BNNTs decreases the energy gaps of the pure BNNTs, and increases their electrical conductivity. These changes upon the adsorption process concern to the sensitivity of the BNNTs toward NO radical.

The calculated amounts of A, I, η, μ, S, ω and ΔN_{max} for all nanotubes studied here are tabulated in Table 3. Ionization energy is a fundamental description of the chemical reactivity of atoms and molecules. High ionization energy indicates high stability and chemical inertness and small ionization energy indicates high reactivity of the atoms and molecules [52]. Comparison of ionization energy

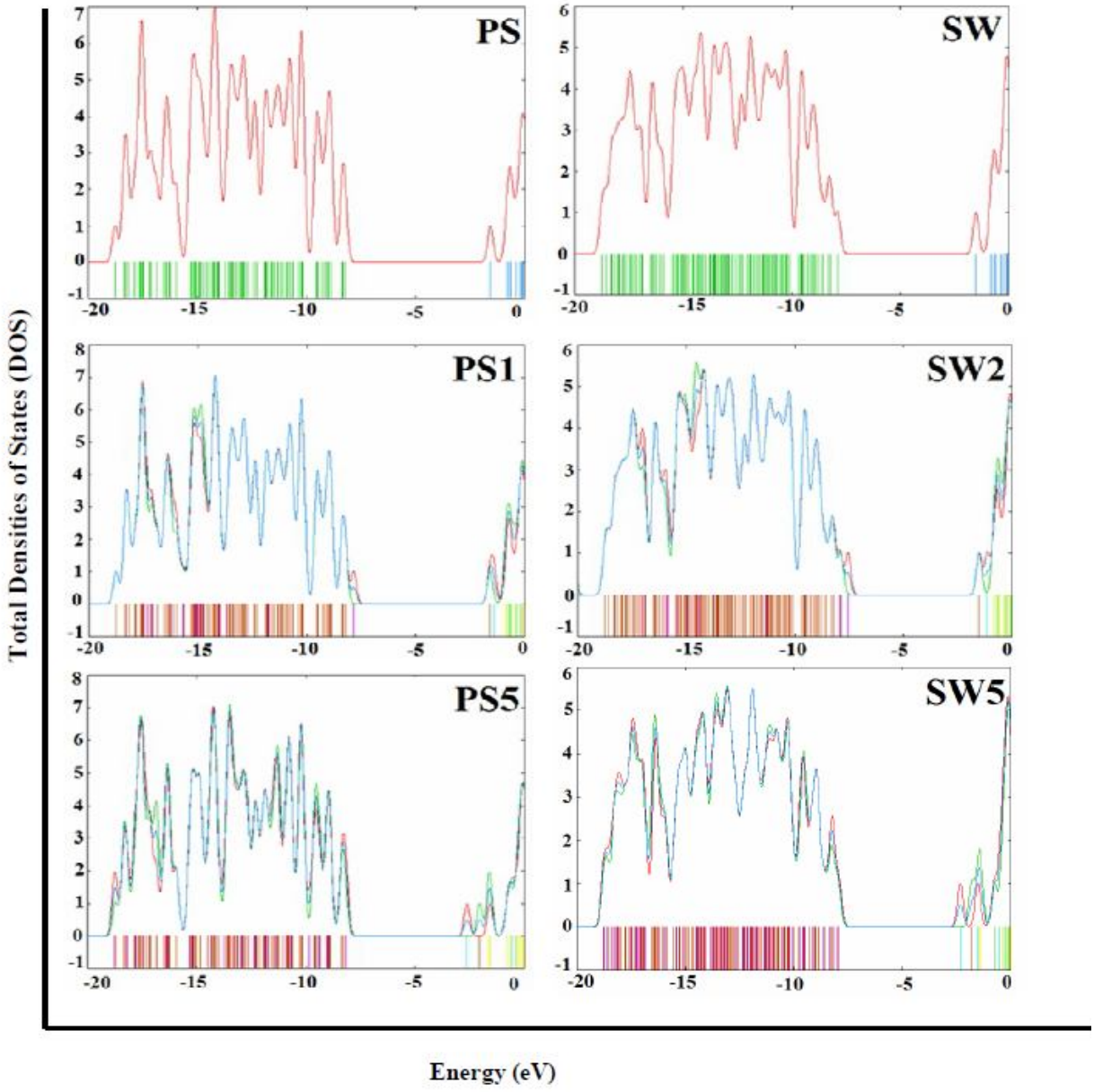

Fig. 4. Density of states (DOS) for different models of the (6,0) BNNTs.

values in Table 3 indicates that I value for pure SW tube is smaller than pure PS (7.88 vs 8.22 eV), so the pure SW nanotube is more reactive than pure PS one. Also, a hard molecule or ion has a large energy gap between the HOMO and LUMO, and a soft molecule or ion has a small energy gap. Soft molecules will also be more polarizable and reactive than hard molecules. Global hardness and softness are of interest, since resistance to change of the electron cloud of a chemical system can be understood from the values of η and S. It was found that stability of chemical species could be associated with its hardness [73]. As shown in Table 3, value of η and S in pure PS-BNNT is 3.32 and 0.15 eV and in pure SW-BNNT is 3.18 and 0.16 eV, respectively. The η value in PS-BNNT is greater than

SW one, indicating that the SW tube is more suitable for NO sensing. In addition, a reagent with high μ is a good electron donor, whereas a reagent with a small μ is a good electron acceptor. The μ and η are generally considered intrinsic properties of a molecule. A molecule with low μ and small η is a good electrophile [74]. The μ values for PS- and SW-BNNTs are -4.90 and -4.70 eV, respectively, indicating that the μ increases slightly upon pure to Stone-Wales transformation. Also, according to the definition of ω, this index measures the propensity of chemical species to accept electrons. The ω values for two BNNTs are in order: PS-BNNT (3.61 eV) > SW-BNNT (3.46 eV). Comparison of values in Table 3 indicates that when NO is adsorbed on outer surface sites of both PS- and SW-BNNTs, energy gap decreases thus η, absolute values of μ and ω values of pure BNNTs decrease and chemical softness as well as ΔN_{max} increases. For internal sites of both PS and SW nanotubes the chemical hardness of the BNNTs decrease and the chemical softness as well as electrophilicity index increases upon adsorption. In addition, the absolute values of chemical potential and ΔN_{max} increase when the NO radical is adsorbed inside of BNNTs. Consequently, adsorption of NO radical by BNNTs is accompanied with the increase in S and ΔN_{max} and decrease in η.

The work function (ϕ) is another critical quantity in understanding the field emission properties of nanotubes. The work function of a surface is the least amount of energy required to remove an electron from the Fermi level to a point far enough not to feel any influence from the surface (or energy needed to move an electron from the Fermi energy level into vacuum) [3]. The magnitude of the work function is usually about a half of the ionization energy of a free atom of the metal. The ionization energy of an atom or molecule, on the other hand, is the energy required to remove one mole of electrons from one mole of isolated gaseous atoms or ions.

The change in the work function of BNNTs after the adsorption of NO radical modifies their field emission properties and it also ascribes to the charge transfer between BNNT surfaces and the NO radical. The emitted electron current densities in vacuum are theoretically described by the following equation

$$j = AT^2 \exp\left(\frac{-\phi}{kT}\right) \quad (2)$$

where A is Richardson constant (A/m^2), T is the temperature (K) and ϕ is the material's work function (eV). Work function values were calculated according to the following equation

$$\phi = E_{inf} - E_F \quad (3)$$

where E_{inf} is the electrostatic potential at infinity and E_F is the Fermi level energy. In this consideration the electrostatic potential at infinity is assumed to be zero. The canonical assumption for position of Fermi level (at T = 0 K) in a molecule is approximately in the middle of the energy gap. It is noteworthy to mention that, in fact, what lies in the middle of the energy gap is the chemical potential, and since the chemical potential of a free gas of electrons is equal to its Fermi level as traditionally defined, herein, the Fermi level of the considered systems is at the center of the energy gap [3]. The calculated work functions of PS- and SW−BNNT are summarized in Table 3. The results reveal that the pure SW-BNNT has lower work function value (3.185 eV) than the pure PS one (3.324 eV). The decrease in the work function upon perfect to Stone-Wales transformation is important for the optoelectronic device design. Also, the work function of both PS- and SW-BNNTs is decreased after adsorption of NO radical. It is expected that the presence of NO radical improves electron emission property of both tubes.

Frontier Molecular Orbitals

The isodensity surfaces of HOMOs and LUMOs of pure nanotubes and their NO adsorptions at internal sites and also in the most stable configurations of outer surface sites (PS1 and SW2) are displayed in Fig. 5. The plots show that for the PS model, the HOMO is quite localized on the nitrogen atoms at the end of N-terminated and corresponds to the lone pair of electron on nitrogen atoms, whereas HOMO in SW-BNNT is localized on the B-N bonds at the defected area and slightly on the nitrogen atoms in the vicinity of the defected region. For both PS and SW tubes, LUMO is more distributed on the B atoms and the B-N pairs along the tube axis at the end of B-terminated. LUMO distribution is

Table 3. The Values of Electron Affinity (A), Ionization Energy (I), Chemical Potential (μ), Chemical Hardness (η), Chemical Softness (S), Electrophilicity Index (ω), Maximum Amount of Electronic Charge (ΔN_{max}) and Work Function (ϕ) of Zigzag BNNTs

Models	A (eV)	I (eV)	μ (eV)	η (eV)	S (eV^{-1})	Ω (eV)	ΔN_{max} (a.u)	ϕ(eV)
Pure PS	1.577	8.225	-4.901	3.324	0.150	3.614	1.475	3.324
PS1	1.577	7.842	-4.709	3.132	0.160	3.540	1.504	3.132
PS2	1.575	7.776	-4.675	3.101	0.161	3.525	1.508	3.101
PS3	1.573	7.813	-4.693	3.120	0.160	3.529	1.504	3.120
PS4	1.577	7.815	-4.696	3.119	0.160	3.535	1.506	3.119
PS5	2.625	8.150	-5.387	2.763	0.181	5.253	1.950	2.792
Pure SW	1.511	7.880	-4.695	3.185	0.157	3.461	1.474	3.185
SW1	1.511	7.637	-4.574	3.063	0.163	3.415	1.493	3.063
SW2	1.509	7.546	-4.528	3.018	0.166	3.396	1.500	3.018
SW3	1.506	7.771	-4.639	3.132	0.160	3.435	1.481	3.132
SW4	1.502	7.793	-4.648	3.146	0.159	3.434	1.478	3.146
SW5	2.333	7.916	-5.124	2.792	0.179	4.703	1.836	2.792
NO	1.459	7.938	-4.698	3.240	0.154	3.407	1.450	3.324

contracted upon perfect to Stone-Wales transformation. For NO adsorbed on outer surface sites of BNNT models, the HOMO is localized on the B-N bond along the tube axis at the end of B-terminated. Based on Fig. 5, LUMO at the outer surface site of PS model is distributed on the B-N bonds along the tube axis at the end of N-terminated and also distributed on the B atoms, whereas for the SW model LUMO is more localized on B-B bond at the defected area and slightly distributed on the B atoms of the SW-BNNT.

For internal sites, the HOMO for the PS model is localized on the O-N bond of NO molecule and on the B-N bond along the tube axis mainly at the end of B-terminated whereas HOMO in SW model is more localized on O-N and B-B bonds and slightly distributed on B-N bonds at the center of the BNNT. In contrast, electron density of LUMO at inside of PS model is more localized on O-N bond and the B-N bond along the tube axis mainly at the center of the BNNT, whereas LUMO for SW-BNNT at internal site is distributed on the B-N bonds along the tube axis at the end of the B-terminal and slightly distributed on N-O bond.

CONCLUSIONS

The optimizations based on DFT/M06-2X method were carried out to examine the adsorption and sidewall reactivity of NO radical on the perfect (PS) and Stone-Wales defected (SW) (6,0) BNNTs. The results show that the NO radical prefers to adsorb on the center site above the hexagon, pentagon or heptagon rings on the outer surface of both PS and SW tubes. Our results indicate that the NO adsorption

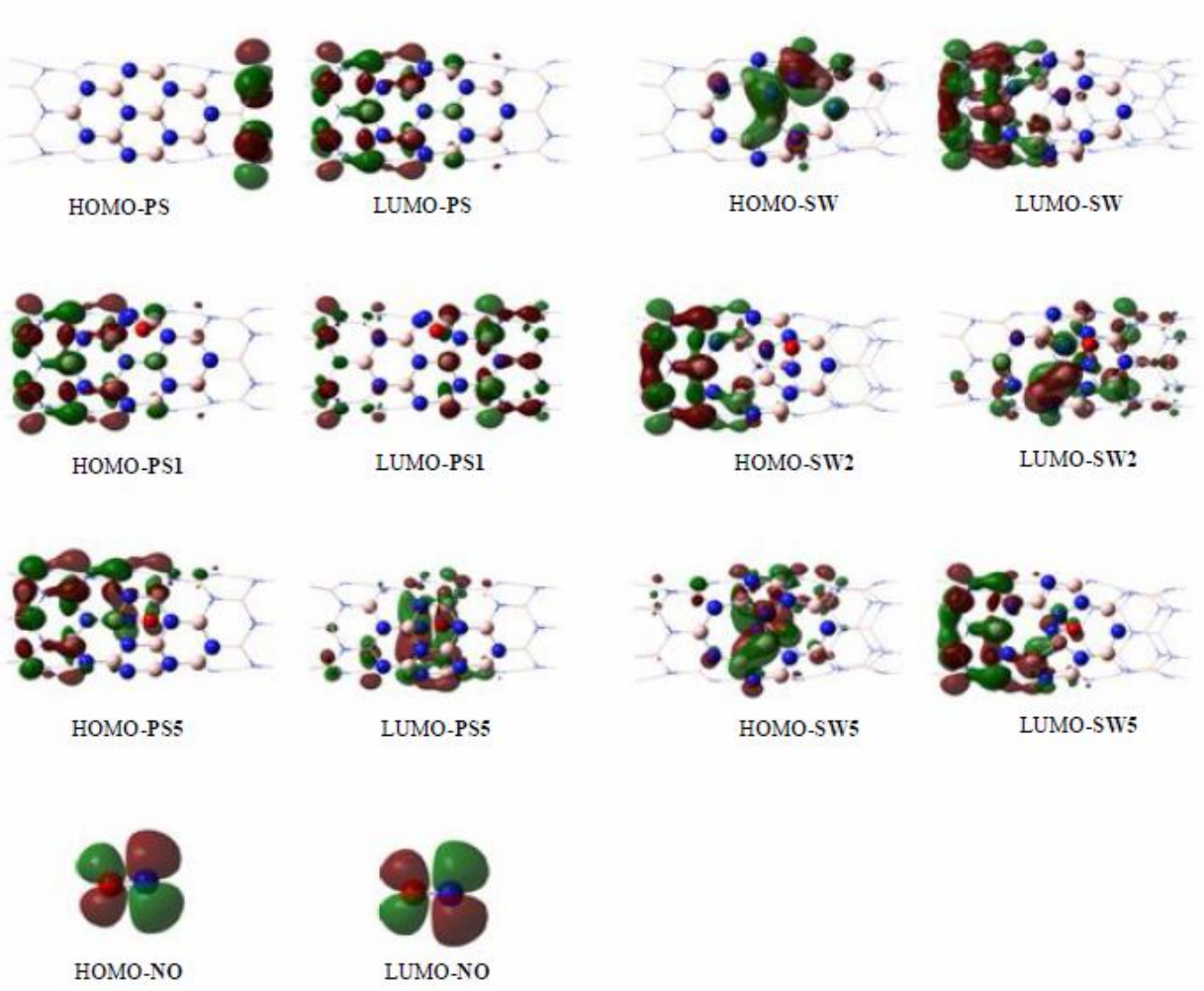

Fig. 5. The isodensity surface of HOMOs and LUMOs for NO and different models of the (6,0) BNNTs at the isovalue of 0.03. O, N and B atoms are represented by red, blue and pink spheres (For interpretation of the references to color in this figure legend, the reader is referred to the web version of this article).

on the outer surface sites of PS- and SW-BNNTs occurs *via* exothermic processes, while for internal site of both PS and SW nanotubes NO adsorption occurs *via* an endothermic process. The analysis of electronic properties indicates that the adsorption of NO on both PS- and SW-BNNTs decreases the energy gap of the BNNTs, and increases their electrical conductance. This fact demonstrates the usefulness of BNNTs for the development of gas sensors. Besides, decrease in energy gap for internal sites of both PS and SW tubes is greater than corresponding outer surface sites. From work function value, it is expected that the presence of NO radical improves electron emission property of both tubes.

REFERENCES

[1] Rubio, A.; Corkill, J. L.; Cohen, M. L., Theory of graphitic boron nitride nanotubes. *Phys. Rev. B* **1994**, *49*, 5081-5084, DOI: 10.1103/PhysRevB.49.5081.

[2] Bai, X.; Golberg, D.; Bando, Y.; Zhi, C.; Tang, C.; Mitome, M., *et al*., Deformation-driven electrical transport of individual boron nitride nanotubes. *Nano Lett*. **2007**, *7*, 632-637, DOI: 10.1021/nl062540l.

[3] Beheshtian, J.; Peyghan, A. A.; Bagheri, Z., Detection

of phosgene by Sc-doped BN nanotubes: a DFT study. *Sens Actuators, B* **2012**, *171*, 846-852, DOI: 10.1016/j.snb.2012.05.082.

[4] Reddy, A. L. M.; Gupta, B. K.; Narayanan, T. N.; Martí, A. A.; Ajayan, P. M.; Walker, G. C., Probing of Ni-encapsulated ferromagnetic boron nitride nanotubes by time-resolved and steady-state photoluminescence spectroscopy. *J. Phys. Chem. C* **2012**, *116*, 12803-12809, DOI: 10.1021/jp210597m.

[5] Watanabe, K.; Taniguchi, T.; Kanda, H., Ultraviolet luminescence spectra of boron nitride single crystals grown under high pressure and high temperature. *Phys. Status Solidi A* **2004**, *201*, 2561-2565, DOI: 10.1002/pssa.200405188.

[6] Watanabe, K.; Taniguchi, T.; Kanda, H., Direct-bandgap properties and evidence for ultraviolet lasing of hexagonal boron nitride single crystal. *Nat. Mater.* **2004**, *3*, 404-409, DOI: 10.1038/nmat1134.

[7] Reddy, A. L. M.; Tanur, A. E.; Walker, G. C., Synthesis and hydrogen storage properties of different types of boron nitride nanostructures. *Int. J. Hydrogen Energy* **2010**, 35, 4138-4143, DOI: 10.1016/j.ijhydene.2010.01.072.

[8] An, W.; Wu, X.; Yang, J. L.; Zeng, X. C., Adsorption and surface reactivity on single-walled boron nitride nanotubes containing stone-wales defects. *J. Phys. Chem. C* **2007**, *111*, 14105-14112, DOI: 10.1021/jp072443w.

[9] Ma, R.; Golberg, D.; Bando, Y.; Sasaki, T., Syntheses and properties of B-C-N and BN nanostructures. *Phil. Trans. R Soc. A* **2004**, *362*, 2161-2186, DOI: 10.1098/rsta.2004.1434.

[10] Terrones, M.; Romo-Herrera, J. M.; Cruz-Silva, E.; López-Urías, F.; Munoz-Sandoval, E.; Velázquez-Salazar, J. J., *et al*., Pure and doped boron nitride nanotubes. *Mater. Today* **2007**, *10*, 30-38, DOI: 10.1016/S1369-7021(07)70077-9.

[11] Stone, A. J.; Wales, D. J., Theoretical studies of icosahedral C60 and some related species. *Chem Phys Lett* **1986**, *128*, 501-503, DOI:10.1016/0009-2614(86)80661-3.

[12] Song, J.; Jiang, H.; Wu, J.; Huang, Y.; Hwang, K. C., Stone-Wales transformation in boron nitride nanotubes. *Scripta Mater*. **2007**, *57*, 571-574, DOI: 10.1016/j.scriptamat.2007.06.027.

[13] Kim, G.; Park, J.; Hong, S., First-principles study of substitutional carbon pair and Stone-Wales defect complexes in boron nitride nanotubes. *Chem. Phys. Lett*. **2012**, *522*, 79-82, DOI: 10.1016/j.cplett.2011.12.001.

[14] Roszer, T., The Biology of Subcellular Nitric Oxide. Springer: 2012. p. 3-21.

[15] Fujitani, T.; Nakamura, I.; Kobayashi, Y.; Takahashi, A.; Haneda, M.; Hamada, H., Adsorption and reactions of NO on clean and CO-precovered Ir (111). *J. Phys. Chem. B* **2005**, *109*, 17603-17607, DOI: 10.1021/jp053092t.

[16] Chang, C. W.; Maduraiveeran, G.; Xu, J. C.; Hunter, G. W.; Dutta, P. K., Design, fabrication, and testing of MEMS-based miniaturized potentiometric nitric oxide sensors. *Sens. Actuators, B* **2014**, *204*, 183-189, DOI: 10.1016/j.snb.2014.06.108.

[17] Yeung, C. S.; Chen, Y. K.; Wang, Y. A. Defected and Substitutionally Doped Nanotubes: Applications in Biosystems, Sensors, Nanoelectronics, and Catalysis. Carbon Nanotubes-Growth and Applications: InTech; 2011. p. 97-132.

[18] Kyotani, T.; Tomita, A., Analysis of the reaction of carbon with NO/N2O using *ab initio* molecular orbital theory. *J. Phys. Chem. B* 1999, *103*, 3434-3441, DOI: 10.1021/jp9845928.

[19] Byl, O.; Kondratyuk, P.; Yates, J. T., Adsorption and Dimerization of NO Inside Single-Walled Carbon Nanotubes An Infrared Spectroscopic Study. *J. Phys. Chem. B* **2003**, *107*, 4277-4279, DOI: 10.1021/jp022565i.

[20] Rafati, A. A.; Hashemianzadeh, S. M.; Nojini, Z. B., Electronic properties of adsorption nitrogen monoxide on inside and outside of the armchair single wall carbon nanotubes: a density functional theory calculations. *J. Phys. Chem. C* **2008**, *112*, 3597-3604, DOI: 10.1021/jp709955g.

[21] Gowrisankar, P. A.; Udhayakumar, K., Electronic properties of boron and silicon doped (10,0) zigzag single-walled carbon nanotube upon gas molecular adsorption: a DFT comparative study. *J. Nanomater.* **2013**, *2013*, 1-12, DOI: 10.1155/2013/293936.

[22] Gao, G.; Kang, H. S., First principles study of NO and

NNO chemisorption on silicon carbide nanotubes and other nanotubes. *J. Chem. Theory Comput*. **2008**, *4*, 1690-1697, DOI: 10.1021/ct800273c.

[23] Baierle, R. J.; Schmidt, T. M.; Fazzio, A., Adsorption of CO and NO molecules on carbon doped boron nitride nanotubes. *Solid State Commun*. **2007**, *142*, 49-53, DOI: 10.1016/j.ssc.2007.01.036.

[24] Xie, Y.; Huo, Y. P.; Zhang, J. M., First-principles study of CO and NO adsorption on transition metals doped (8,0) boron nitride nanotube. *Appl. Surf. Sci*. **2012**, *258*, 6391-6397, DOI: 10.1016/ j.apsusc.2012.03.048.

[25] Roohi, H.; Maleki, L., Effects of C1-3-doping on electronic and structural properties of Stone-Wales defective boron nitride nanotubes as well as their NO gas sensitivity. *RSC Adv.***2016**, *6,* 11353-11369, DOI: 10.1039/C5RA20920J.

[26] Vreven, T.; Morokuma, K., On the application of the IMOMO (integrated molecular orbital+molecular orbital) method. *J. Comput. Chem*. **2000**, *21*, 1419-1432, DOI: 10.1002/1096-987X(200012)21:16< 1419:AID-JCC1>3.0.CO;2-C.

[27] Torrent, M.; Vreven, T.; Musaev, D. G.; Morokuma, K.; Farkas, Ö.; Schlegel, H. B., Effects of the protein environment on the structure and energetics of active sites of metalloenzymes. ONIOM study of methane monooxygenase and ribonucleotide reductase. *J. Am. Chem. Soc.* **2002**, *124*, 192-193 DOI: 192-193, 10.1021/ja016589z.

[28] Svensson, M.; Humbel, S.; Froese, R. D.; Matsubara, T.; Sieber, S.; Morokuma, K., ONIOM: A multilayered integrated MO+ MM method for geometry optimizations and single point energy predictions. A test for Diels-Alder reactions and Pt (P (t-Bu) 3) 2+H_2 oxidative addition. *The Journal of Phys. Chem*. **1996**, *100*, 19357-19363, DOI: 10.1021/ jp962071j.

[29] Vreven, T.; Byun, K. S.; Komáromi, I.; Dapprich, S.; Montgomery, J. A.; Morokuma, K., *et al*., Combining quantum mechanics methods with molecular mechanics methods in ONIOM. *J. Chem. Theory Comput*. **2006**, *2*, 815-826, DOI: 10.1021/ ct050289g.

[30] Vreven, T.; Thompson, L. M.; Larkin, S. M.; Kirker, I.; Bearpark, M. J., Deconstructing the ONIOM Hessian: investigating method combinations for transition structures. *J. Chem. Theory Comput*. **2012**, *8*, 4907-4914, DOI: 10.1021/ct300612m.

[31] Schatz, G. C., Using theory and computation to model nanoscale properties. *Proceedings of the National Academy of Sci.* **2007**, *104*, 6885-6892, DOI: 10.1073/ pnas.0702187104.

[32] 32- Wang, L.; Yi, C.; Zou, H.; Gan, H.; Xu, J.; Xu, W., Initial reactions of methyl-nitramine confined inside armchair (5,5) single-walled carbon nanotube. *J. Mol. Model* **2011**, 17, 2751-2758, DOI: 10.1007/ s00894-011-0967-x.

[33] Basiuk, V. A., ONIOM studies of chemical reactions on carbon nanotube tips: effects of the lower theoretical level and mutual orientation of the reactants. *J. Phys. Chem. B* **2003**, *107*, 8890-8897, DOI: 10.1021/jp034829m.

[34] Kar, T.; Akdim, B.; Duan, X.; Pachter, R., A theoretical study of functionalized single-wall carbon nanotubes: ONIOM calculations. *Chem. Phys. Lett.* **2004**, *392*, 176-180, DOI: 10.1016/ j.cplett.2004.05.015.

[35] Lu, X.; Tian, F.; Zhang, Q., The [2+1] cycloadditions of dichlorocarbene, silylene, germylene, and oxycarbonylnitrene onto the sidewall of armchair (5, 5) single-wall carbon nanotube. *J. Phys. Chem. B* **2003**, *107,* 8388-8391, DOI: 10.1021/jp034820k.

[36] Liu, L. V.; Tian, W. Q.; Wang, Y. A., Ozonization at the vacancy defect site of the single-walled carbon nanotube. *J. Phys. Chem. B* **2006**, *110*, 13037-13044, DOI: 10.1021/jp055999x.

[37] Tetasang, S.; Keawwangchai, S.; Wanno, B.; Ruangpornvisuti, V., Quantum chemical investigation on structures of pyrrolic amides functionalized (5,5) single-walled carbon nanotube and their binding with halide ions. *Struct. Chem.* **2012**, *23*, 7-15, DOI: 10.1007/s11224-011-9839-3.

[38] Lu, X.; Tian, F.; Wang, N.; Zhang, Q., Organic functionalization of the sidewalls of carbon nanotubes by Diels-Alder reactions: a theoretical prediction. *Org. lett.* **2002**, *4*, 4313-4315, DOI: 10.1021/ ol026956r.

[39] Basiuk, V. A., Reactivity of carboxylic groups on armchair and zigzag carbon nanotube tips: a

theoretical study of esterification with methanol. *Nano Lett.* **2002**, *2*, 835-839, DOI: 10.1021/nl025607n.

[40] Xu, Y. J.; Li, J. Q., The interaction of N_2 with active sites of a single-wall carbon nanotube. *Chem. Phys. Lett.* **2005**, *412*, 439-443, DOI: 10.1016/ j.cplett.2005.07.053.

[41] Ahmadi, A.; Beheshtian, J.; Hadipour, N. L., Chemisorption of NH3 at the open ends of boron nitride nanotubes: a DFT study. *Struct. Chem.* **2011**, *22*, 183-188, DOI: 10.1007/s11224-010-9697-4.

[42] Zhao, Y.; Truhlar, D. G., The M06 suite of density functionals for main group thermochemistry, thermochemical kinetics, noncovalent interactions, excited states, and transition elements: two new functionals and systematic testing of four M06-class functionals and 12 other functionals. *Theor. Chem. Acc.* **2008**, *120*, 215-241, DOI: 10.1007/s00214-007-0310-x.

[43] Ditchfield, R.; Hehre, W. J.; Pople, J. A., Self-consistent molecular-orbital methods. IX. An extended Gaussian-type basis for molecular-orbital studies of organic molecules. *J. Chem. Phys.* **1971**, *54*, 724-728, DOI: 10.1063/1.1674902.

[44] Hehre, W. J.; Ditchfield, R.; Pople, J. A., Self-consistent molecular orbital methods. XII. Further extensions of gaussian-type basis sets for use in molecular orbital studies of organic molecules. *J. Chem. Phys.* **1972**, *56*, 2257-2261, DOI: 10.1063/ 1.1677527.

[45] Hariharan, P. C.; Pople, J. A., The influence of polarization functions on molecular orbital hydrogenation energies. *Theoretica Chim. Acta* **1973**, *28*, 213-222, DOI: 10.1007/BF00533485.

[46] Stewart, J. J. P., Optimization of parameters for semiempirical methods V: modification of NDDO approximations and application to 70 elements. *J. Mol. Model.* **2007**, *13*, 1173-1213, DOI: 10.1007/ s00894-007-0233-4.

[47] Pearson, R. G., Absolute electronegativity and hardness: applications to organic chemistry. *J. Org. Chem.* **1989**, *54*, 1423-1430, DOI: 10.1021/ jo00267a034.

[48] Parr, R. G.; Zhou, Z., Absolute hardness: unifying concept for identifying shells and subshells in nuclei, atoms, molecules, and metallic clusters. *Acc. Chem. Res.* **1993**, *26*, 256-258, DOI: 10.1021/ar00029a005.

[49] Koopmans, T., Über die Zuordnung von Wellenfunktionen und Eigenwerten zu den einzelnen Elektronen eines Atoms. *Physica* **1934**, *1*, 104-113, DOI: 10.1016/S0031-8914(34)90011-2.

[50] Pearson, R. G., Chemical hardness and density functional theory. *J. Chem. Sci.* **2005**, *117*, 369-377, DOI: 10.1007/BF02708340.

[51] Parr, R. G.; Szentpály, L.; Liu, S., Electrophilicity index. *J. Am. Chem. Soc.* **1999**, *121*, 1922-1924, DOI: 10.1021/ja983494x.

[52] Babu, N. S.; Tadeasse, S.; Lelisho, T. A.; Padmaja, N., Theoretical studies of stability, and local molecular properties of allopurinol isomers by density Functional theory. *IJPRS* **2014**, *3*, 557-565.

[53] Frisch, M.; Trucks, G. W.; Schlegel, H. B.; Scuseria, G. E.; Robb, M. A.; Cheeseman, J. R., *et al.*, Gaussian 03, revision c. 02; Gaussian. Inc, Wallingford, CT 2004, 4.

[54] Schmidt, M. W.; Baldridge, K. K.; Boatz, J. A.; Elbert, S. T.; Gordon, M. S.; Jensen, J. H., et al., General atomic and molecular electronic structure system. *J. Comput. Chem.* **1993**, *14*, 1347-1363, DOI: 10.1002/jcc.540141112.

[55] O'boyle, N. M.; Tenderholt, A. L.; Langner, K. M., Cclib: a library for package-independent computational chemistry algorithms. *J. Comput. Chem.* **2008**, *29*, 839-845, DOI: 10.1002/jcc.

[56] Miyamoto, Y.; Rubio, A.; Berber, S.; Yoon, M.; Tománek, D., Spectroscopic characterization of Stone-Wales defects in nanotubes. *Phys. Rev. B* **2004**, *69*, 121413, DOI: 10.1103/PhysRevB.69.121413.

[57] 57- Li, Y.; Zhou, Z.; Golberg, D.; Bando, Y.; Schleyer, P. V. R.; Chen, Z., Stone-Wales defects in single-walled boron nitride nanotubes: formation energies, electronic structures, and reactivity. *J. Phys. Chem. C* **2008**, *112*, 1365-1370, DOI: 10.1021/jp077115a.

[58] 58- Srivastava, D.; Menon, M.; Cho, K. J., Anisotropic nanomechanics of boron nitride nanotubes: Nanostructured "skin" effect. *Phys. Rev. B* **2001**, *63*, 195413, DOI: 10.1103/ PhysRevB.63.195413.

[59] Menon, M.; Srivastava, D., Structure of boron nitride nanotubes: tube closing versus chirality. *Chem. Phys. Lett.* **1999**, *307*, 407-412, DOI: 10.1016/S0009-2614(99)00552-7.

[60] Beheshtian, J.; Kamfiroozi, M.; Bagheri, Z.; Ahmadi, A., Computational study of CO and NO adsorption on magnesium oxide nanotubes. *Physica E* **2011**, *44*, 546-549, DOI: 10.1016/j.physe.2011.09.016.

[61] Dai, J.; Giannozzi, P.; Yuan, J., Adsorption of pairs of NOx molecules on single-walled carbon nanotubes and formation of NO+ NO3 from NO_2. *Surf Sci* **2009**, *603*, 3234-3238, DOI: 10.1016/ j.susc.2009.09.010.

[62] Vasylenko, A. I.; Tokarchuk, M. V.; Jurga, S., Effect of a vacancy in single-walled carbon nanotubes on He and NO adsorption. J. Phys. Chem. C **2015**, 119, 5113-5116, DOI: 10.1021/jp511532j.

[63] El-Barbary, A. A.; Eid, K. M.; Kamel, M. A.; Taha, H. O.; Ismail, G. H., Adsorption of CO, CO2, NO and NO2 on Boron Nitride Nanotubes: DFT Study. *Journal of Surface Engineered Materials and Advanced Technology* **2015**, *5*, 154-161, DOI: 10.4236/jsemat.2015.53017

[64] Hohenstein, E. G.; Chill, S. T.; Sherrill, C. D., Assessment of the performance of the M05− 2X and M06-2X exchange-correlation functionals for noncovalent interactions in biomolecules. *J. Chem. Theory Comput.* **2008**, *4,* 1996-2000, DOI: 10.1021/ct800308k.

[65] 65- Zhao, Y.; Schultz, N. E.; Truhlar, D. G., Exchange-correlation functional with broad accuracy for metallic and nonmetallic compounds, kinetics, and noncovalent interactions. *J. Chem. Phys.* **2005**, *123*, 161103/161101-161103/161104, DOI: 10.1063/ 1.2126975.

[66] Zhao, Y.; Schultz, N. E.; Truhlar, D. G., Design of density functionals by combining the method of constraint satisfaction with parametrization for thermochemistry, thermochemical kinetics, and noncovalent interactions. *J. Chem. Theory Comput.* **2006**, *2*, 364-382, DOI: 10.1021/ct0502763.

[67] Zhao, Y.; Truhlar, D. G., A new local density functional for main-group thermochemistry, transition metal bonding, thermochemical kinetics, and noncovalent interactions. *J. Chem. Phys.* **2006**, *125*, 194101/194101–194101/194118., DOI: 10.1063/ 1.2370993.

[68] Zhao, Y.; Truhlar, D. G., Density functionals for noncovalent interaction energies of biological importance. *J. Chem. Theory Comput.* **2007**, *3*, 289-300, DOI: 10.1021/ct6002719.

[69] Perdew, J. P.; Burke, K.; Ernzerhof, M., Generalized gradient approximation made simple. *Phys. Rev. Lett.* **1996**, 77, 3865-3868, DOI: 10.1103/ PhysRevLett.77.3865.

[70] Jurečka, P.; Šponer, J.; Černý, J.; Hobza, P., Benchmark database of accurate (MP2 and CCSD (T) complete basis set limit) interaction energies of small model complexes, DNA base pairs, and amino acid pairs. *Phys. Chem. Chem. Phys.* **2006**, *8*, 1985-1993, DOI: 10.1039/B600027D.

[71] Gu, J.; Wang, J.; Leszczynski, J.; Xie, Y.; Schaefer III, H. F., To stack or not to stack: performance of a new density functional for the uracil and thymine dimers. *Chem. Phys. Lett.* **2008**, *459*, 164-166, DOI: 10.1016/j.cplett.2008.05.049.

[72] Beheshtian, J.; Baei, M. T.; Peyghan, A. A., Theoretical study of CO adsorption on the surface of BN, AlN, BP and AlP nanotubes. *Surface Sci.* **2012**, *606*, 981-985, DOI: 10.1016/ j.susc.2012.02.019.

[73] Pearson, R. G., Recent advances in the concept of hard and soft acids and bases. *J. Chem. Educ.* **1987**, *64*, 561-567, DOI: 10.1021/ed064p561.

[74] Ayers, P. W.; Anderson, J. S.; Bartolotti, L. J., Perturbative perspectives on the chemical reaction prediction problem. *Int. J. Quantum Chem.* **2005**, *101*, 520-534, DOI: 10.1002/qua.20307.